Manipulation of Microparticles in Optofluidic Devices Fabricated by Femtosecond Laser Micromachining

Carolina Cameira[1,2*], *João M. Maia*[2], *and P. V. S. Marques*[1,2]

[1]Department of Physics and Astronomy, Faculty of Sciences of University of Porto, 4169-007 Porto, Portugal
[2]CAP – Centre for Applied Photonics, INESC TEC, 4150-179 Porto, Portugal

Abstract. This study reports the fabrication of three-dimensional microfluidic channels in fused silica, using femtosecond laser micromachining, to achieve two-dimensional hydrodynamic flow focusing in either the horizontal or the vertical directions. Spatial focusing of 3 μm polystyrene particles was successfully demonstrated, showing the ability of the fabricated devices to confine microparticles within a 6 μm layer over a channel width of 420 μm and within a 5 μm layer over a channel height of 260 μm. Integration of laser-direct written optical waveguides inside a microfluidic chip and orthogonal to the channel also enabled the implementation of a dual-beam optical trap, with trapping of polystyrene microparticles using a 1550 nm beam being demonstrated.

1 Introduction

In the past decade, LOC (lab-on-a-chip) devices have proven to be a powerful and reliable biosensing technology for medical and healthcare applications, offering benefits such as point-of-care diagnostics, faster analysis times, reduced reagent costs, and less chemical waste [1]. LOC technology integrates multiple functions (fluidic, optical, electrochemical, …) onto a single chip with mm^2 footprint, enhancing the automation, compactness, and portability of these devices.

LOC devices have traditionally been fabricated by planar processes, such as photolithography and soft lithography. However, the manufacturing of 3D structures through these microfabrication techniques is considerably complex and time-consuming, given that these require stacking of multiple 2D structures. Another promising method for fabricating LOC devices is femtosecond (fs) laser micromachining. This technique, which can be applied to a wide range of materials transparent to the laser wavelength, relies on non-linear absorption of the pulsed laser beam and relaxation processes to alter the material properties at the laser beam's focal point [2]. For instance, fs-laser exposure in fused silica can induce a refractive index increase or higher etching rate in HF acid [3]. Besides its capability for 3D machining, this technique also permits the integration of both optical and fluidic functions on a single chip [4]. It enables the development of devices leading to processing of fluidic samples—such as cell imaging [5], fluid mixing [6], particle separation or focusing [7]—as well as their analysis through optical trapping [8], fluorescence [9], and backscattered light [10].

Here, fs-laser micromachining is used to fabricate optical waveguides and 3D microfluidic channels in a single chip to develop a flow cytometry device for optical manipulation and analysis of microparticles and cells. To achieve single-particle level sensing, it is fundamental to have precise control over particle movement and positioning within the channels [11]. For this reason, we design microfluidic channels with a three-dimensional geometry capable of controlling the distribution of microparticles both horizontally and vertically through hydrodynamic flow focusing (HFF), by adjusting the ratio between sheath and sample flow rates. On-chip integration of optical waveguides towards microparticle/cell optical sensing is also demonstrated through the creation of a 1550 nm dual-beam optical trap.

2 Experimental Methods

2.1 Fabrication

A fiber amplified diode pumped ultrafast laser (Amplitude Systèmes Satsuma HP) operating at 515 nm and emitting 250 fs long pulses at 500 kHz was used to either induce an increase of the refractive index or of the chemical etching rate in 30×25×1 mm^3 fused silica (Suprasil 1) substrates. The linearly polarized laser beam was focused inside the substrate via a 0.42 NA objective (Mitutoyo M Plan Apo NIR 50x). The substrate is held in place by vacuum on a stainless-steel sample holder, which in turn is set on top of Aerotech direct-drive translation stages for controlled movement along the XY plane (ANT130XY-110 PLUS) and along the Z direction (ANT130V-5 PLUS). Stage movement,

*Corresponding author: carolina.cameira@inesctec.pt

as well as pulse energy and polarisation, are all controlled with the Workshop of Photonics workstation's SCA software.

Optical waveguides are directly written by translating the substrate along the XY plane relative to the laser focus, with the laser beam polarisation parallel to the scanning direction.

The microfluidic channel fabrication is more intricate since it requires the programming of more complex 3D geometries. These are directly programmed in the SCA software interface, with the 3D object being sliced and hatched into a set of linearly spaced laser-tracks that are scanned sequentially from bottom-to-top with the laser beam polarization always perpendicular to the scanning direction for a more effective chemical etching rate increase. Chemical etching is performed by immersing the substrate in hydrofluoric acid (HF) at either a 10% or 20% volume concentration in an ultrasonic bath inside an ISO-6/7 clean room facility. Typical surface roughness values of the fabricated microchannels are around 90 nm. This result was obtained in a separate study using the same laser direct writing and chemical etching systems, similar materials and processing parameters [12]. The surface roughness can be reduced through thermal annealing [12], oxyhydrogen flame heating [13] or CO2 laser irradiation [14]. In between steps, the substrate side facets are mechanically polished to suppress the waveguide tapered end region arising due to the laser failing to converge to a single focal spot at the interface.

Lastly, a polydimethylsiloxane (PDMS) layer is fabricated, pierced with a blunt-end steel syringe needle to fit the capillary tubes (Darwin Microfluidics, PTFE Tubing 1/16” OD - 0.5mm) used for fluid injection or withdrawal, and plasma-bonded to the fused silica chip to seal the microfluidic device.

2.1.1 Horizontal HFF Device

A scheme of the device is depicted in figure 1. The microfluidic channel has three inlets, one for the sample and two for the sheath solutions, and one outlet. The sample and sheath flows intersect at a 90º angle. The main channel has a square cross-section measuring 400×250 μm^2 (width by height), and the diameter of the inlets/outlets is 1.2 mm. The other dimensions are indicated in fig. 1.

The 3D channel was sliced into 5 μm spaced layers, which were then hatched into linear tracks with a period of 10 μm. Each track was written with a pulse energy of 125 nJ at 5 mm/s. The etching step for the channel fabrication took two hours and fifteen minutes with a 20% HF volume concentration. Microfluidic channel width and height increased by 20 and 10 μm, respectively, during chemical etching.

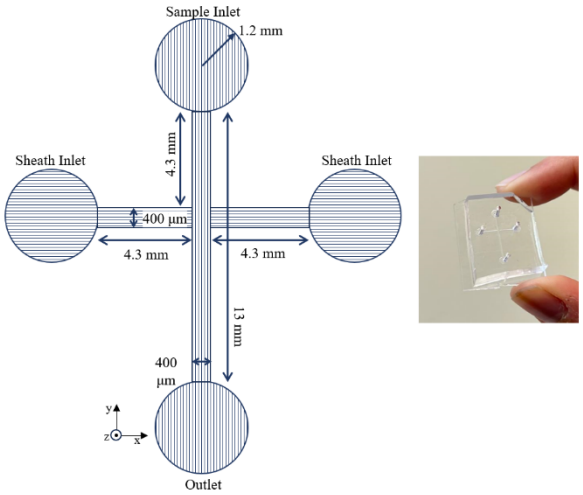

Fig. 1. Top view schematic of the fabricated device to test horizontal HFF (left) and an image of the device (right). Schematic not to scale.

2.1.2 Vertical HFF Device

The device geometry is shown in figure 2. The microfluidic channel contains two inlets, for sample and sheath flows, and an outlet. The sheath flow divides into two subchannels, one at the surface of the chip and another inside it. The sample flow is enclosed by these two subchannels and runs co-directional to them. All dimensions are indicated in fig. 2. During initial trials, it was observed that, despite the symmetric design of the two sheath flow subchannels, these became asymmetric after the etching process. To address this issue, the programmed geometry was adjusted to include slight differences in the dimensions of the subchannels, as illustrated in figure 2. Although this modification mitigated the problem, it did not completely resolve it. Further discussion on the extent of this attenuation will be provided later in the experimental results section.All subchannels have a common width of 400 μm, the sheath subchannels have heights of 52 and 36 μm, the sample subchannel narrows down to a height of 36 μm right before the intersection, and the channel depth is 262 μm after the intersection.

The 3D channel was sliced into 5 μm spaced layers, which were then hatched into linear tracks with a period of 4 and 25 μm for the main channel and inlet/outlet, respectively. Each track was written with a pulse energy of 60 nJ at 5 mm/s. The etching step for the channel fabrication took two hours with a 20% HF volume concentration. During chemical etching, the channel width and height increased by 20 and 10 μm, respectively, and the sheath subchannels became asymmetric, as will be discussed further ahead.

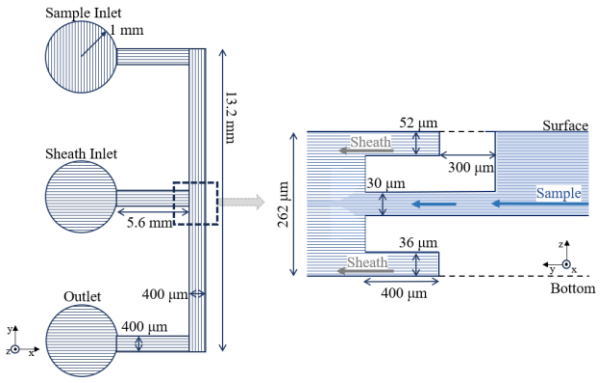

Fig. 2. Top view (left) and side view (right) schematic representation of fabricated device to test vertical HFF. Schematic not to scale.

2.1.3 Dual-Beam Optical Trap Optofluidic Device

The device, shown in figure 3, is composed of a microfluidic channel with one inlet and an outlet for fluid flow with several waveguides crossing the main channel. The microfluidic channel has a depth of 100 µm, the diameter of the circular inlet/outlet is 1.5 mm, and the main channel is 14 mm long and 36 µm wide. The 3D channel was sliced into 5 µm spaced layers, which were then hatched into linear tracks with a period of 2.5 and 5 µm for the main channel and inlet/outlet, respectively. Each track was written with a pulse energy of 60 nJ at 2 mm/s. The etching step for the channel fabrication took one hour and a half with a 10% HF volume concentration.

The optical waveguides were laser-written after chemical etching with a pulse energy of 100 nJ at 200 µm/s. These were written at varying depths covering the channel depth, from 90 to 30 µm with a pitch of 5 µm. Afterwards, the substrate facets are mechanically polished and a V-groove assembly containing an SMF28 fiber is aligned with the 50-µm deep laser written waveguide and bonded to the substrate using UV-cured Norland 81 optical adhesive.

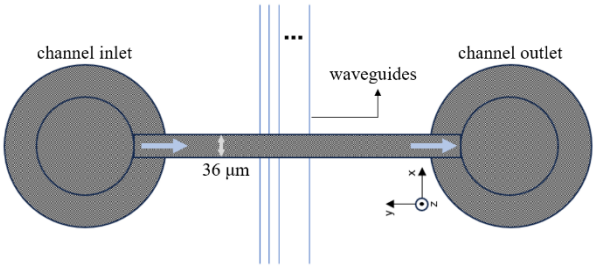

Fig. 3. Top view schematic representation of the optofluidic device with the microfluidic channel integrated with perpendicular optical waveguides. Despite several waveguides being written, only one was used for testing the device. Schematic not to scale.

2.2 Device Characterization

All devices were characterized using red food dye and/or non-functionalized 3-µm spherical polystyrene (PS) particles (Phosphorex, PolySciences) packaged in a 2.7% solids (w/v) aqueous suspension and subsequently diluted in deionized water. The flow rates were controlled by syringe pumps (SP210iw Syringe Pump; AL-4000 Two-Channel Syringe Pump), where the syringes (3 mL plastic B-D; 0.5 and 1 mL glass Hamilton Gastight) were placed and connected to the capillary tubes. Choice of the syringes depends on the used flow rate; lower-volume syringes provide more stability at lower flow rates. A homemade microscope system (employing either one of the following objectives 0.40 NA 20x Olympus ULWD, 0.25 NA 10x Nikon, and 0.10 NA 4x Nikon) was used to record live images of the samples passing through the microfluidic channels via a CCD camera (Thorlabs CS165CU/M Zelux).

3 Experimental Results and Discussion

3.1 Hydrodynamic Flow Focusing

3.1.1 Horizontal Focusing

The device to test horizontal HFF (fig. 1) was firstly tested using deionized water in the two sheath inlets and red food dye diluted in deionized water in the sample inlet, making it possible to observe flow focusing of the sample fluid. Both sheath inlets were connected to the same syringe pump, with 3 mL syringes, so that the sheath's flow rate, Q, was always the same for both inlets, since the channels are symmetrical. On the other hand, the sample fluid flow rate, q, is controlled by another syringe pump, with a 1 mL syringe. This allows the control of the ratio between the sample and sheath flow rate, f = q/2Q, which in turn determines the ratio between the width of the focused sample stream, Wf, and the total width of the channel, W (fig. 4).

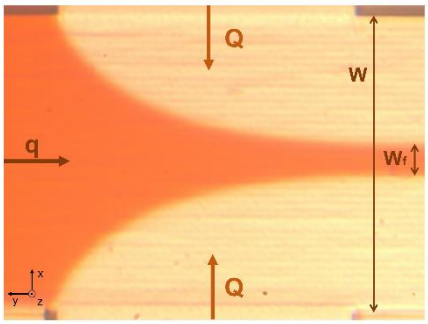

Fig. 4. Image of 2D hydrodynamic focusing on the channel junction of the fabricated device. The total flow rate after the intersection is q+2Q. Image was taken for Q = 20 µL/min and q=5µL/min (f=0.125).

The flow rates Q and q were varied from 10 to 40 µL/min and 1 to 80 µL/min, respectively. Images of the channel were taken at distances ranging from 280 to 380 µm from the centre of the junction and analysed using ImageJ to calculate the ratio between the width of the focused sample stream and the total channel width (Wf/W). This region was selected because the hydrodynamic entrance length for laminar flow, which is the distance at which the fluid's velocity profile becomes fully developed [15], ranges from 6.6 to 89.2 µm under the conditions of this study, thus ensuring that the fluid is fully developed in the measurement region.

Additionally, longer distances were avoided to minimize potential issues arising from diffusion effects. The experimental results are depicted in figure 5. Wf was measured 3 times for each experimental condition, with the resulting standard deviation depicted as an error bar. The dashed lines represent the theoretical results obtained from Lee *et al* [16].

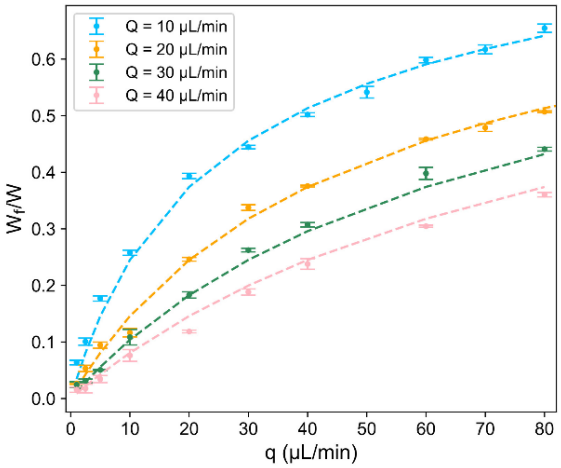

Fig. 5. Experimental results of the variation of the ratio between the focused sample stream width and the total width of the channel, Wf/W, with the sample flow rate, q, for constant sheath flow rates, Q. The dashed lines represent the corresponding theoretical results.

The obtained results follow the expected theoretical behaviour. For a constant sheath flow rate Q, the width of the focused sample stream, Wf, increases as the sample flow rate q is increased. In the extreme condition where Q=0 (no sheath flow) the food dye fills the entire channel. On the other hand, for a constant q, a decrease on the flow rate Q increases the width of the focused sample stream.

Tests with microparticles diluted in water were also performed. Since the diffusion coefficient of PS particles suspended in water is approximately three orders of magnitude lower than that of the food dye [17, 18], it was possible to use lower flow rates, decreasing the particles' flow velocity and thereby facilitating the analysis. In order to test the spatial focusing efficiency of microparticles in the device, their position distribution along the channel was obtained through image analysis using ImageJ. The results for two different flow rate ratios are depicted in figure 6.

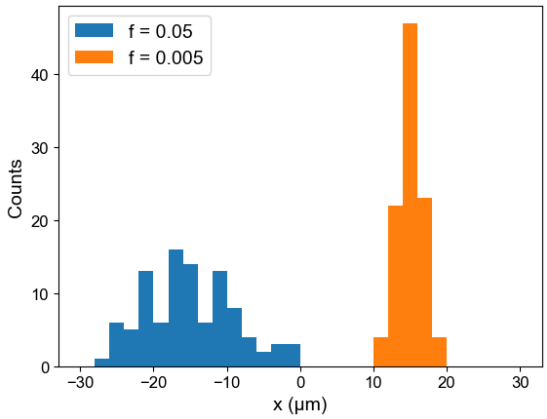

Fig. 6. Histogram of the position of the PS particles along the channel's width for f=0.05 and f=0.005, centered at x = -15 and 15 µm, respectively. The particle solution flow rate was q = 0.05 µL/min for both histograms.

When the sample flow rate, q, is kept constant while the sheath flow rate, Q, is varied, resulting in a change in the flow rate ratio, f, the focused stream width, Wf clearly increases as f increases. Furthermore, considering the width confining 90% of the measured particle position, it was shown that by employing a flow rate ratio of 0.005 it was possible to spatially confine the PS particles within a 6 µm thick layer. Smaller flow rate ratios result in a narrower focal spot, whereas smaller ratios lead to a more dispersed microparticle solution. In the context of this work, the more spatially focused the particles are, the easier it will be to use light to interact with the microparticles and to perform single-particle analysis.

The presented study proved the capability of the fabricated device for horizontal two-dimensional HFF. However, here the focusing was only performed in one direction meaning that the particles can still freely move vertically within the channel. To meticulously achieve single-particle measurements it is crucial to confine the particles in all directions, both in horizontal and vertical directions.

3.1.2 Vertical Focusing

Similarly to the tests performed to test the horizontal HFF, the microfluidic device to test vertical HFF (fig. 2) was firstly tested using deionized water in the sheath inlet and red food dye diluted in deionized water in the sample inlet, which makes it possible to observe flow focusing of the sample fluid. The sheath inlet was connected to a syringe pump, with 1 mL glass syringes, allowing the control of the sheath's flow rate, Q_1+Q_2. On the other hand, the sample fluid flow rate, q, was controlled by another syringe pump, with an identical 1 mL syringe. This allows the control of the ratio between the sample and sheath flow rate, $f = q/(Q_1+Q_2)$, which in turn determines the ratio between the height of the focused sample stream, Hf, and the total height of the channel, H (fig. 7).

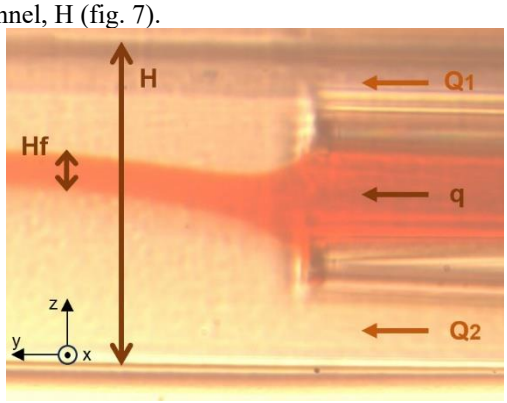

Fig. 7. Image of 2D vertical hydrodynamic focusing on the fabricated device. The total flow rate after the junction is $q+(Q_1+Q_2)$. Image was taken for (Q_1+Q_2) = 100 µL/min and q = 10 µL/min (f=0.1).

As shown in figure 7, the sample fluid is vertically displaced to the centre. This derives from a limited

etching selectivity, which means that the subchannel at the glass surface is etched for a longer period than the bottom subchannel, resulting in two sheath subchannels of different heights and, in turn, different flow rates. This asymmetry affects the overall performance of the device, since the total flow rate (Q_1+Q_2) is not equally distributed between the two sheath subchannels. Consequently, the height of the focused stream can vary based on its position across the channel height, since the stream-wise velocity profile may not be uniform. In order to study the vertical flow focusing, the obtained results were analysed and compared to the asymmetric hydrodynamic flow focusing model, developed by Lee *et al* [16]. This model considers the position of the focused stream, giving rise to more accurate analysis, even though it was developed for a T-junction channel.

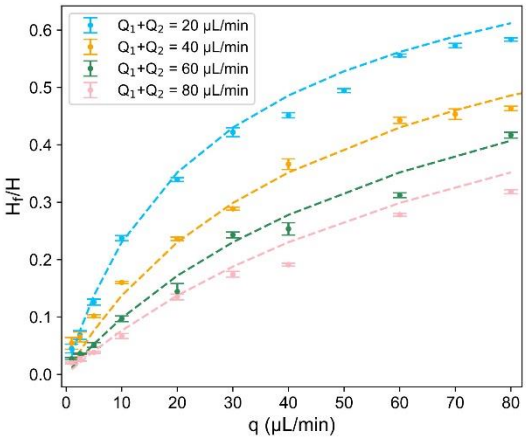

Fig. 8. Experimental results of the variation of the ratio between the focused sample stream height and the total height of the channel, H_f/H, with the sample flow rate, q, for constant sheath flow rates, Q_1+Q_2. The dashed lines represent the corresponding analytical results predicted by Lee's model.

Similarly to the analysis for the horizontal 2D flow focusing, images of the channel were taken and subsequently analysed using the software ImageJ. The experimental results are depicted in figure 8. H_f was measured 3 times for each experimental condition, with the resulting standard deviation depicted as an error bar. The dashed lines represent the analytical results calculated using Lee's asymmetric hydrodynamic flow focusing model, following a similar approach as was used for the study of horizontal HFF.

Again, the tendency of the obtained results follows the expected theoretical behaviour. When the sheath flow rate is kept constant, the height of the focused sample stream, Hf, increases as the sample flow rate is increased. For a constant q, a decrease on the sheath flow rate increases the height of the focused sample stream. It is also worth noting that here, in comparison to the results obtained for the horizontal flow focusing, the experimental errors are considerably higher. This occurs because the etching step significantly impacts the device's geometry, particularly in the vertical direction, which in turn affects flow focusing. Besides, here the angle between the channels was 0º, unlike the 90º angle used in the horizontal focusing device. This difference also contributes to deviations in focusing [19].

Further tests were conducted with PS microparticles. The particle positions along the channel were determined, and the resulting histograms are shown in figure 9. The presented results confirm the capability of the fabricated device to spatially focus particles on the vertical direction inside the channel, with the height of the focused sample stream depending on the flow rate ratio. Particularly, considering the height confining 90% of the measured particle position, by employing a flow rate ratio of 0.005 it is possible to spatially confine the microparticles to a height of around 5 µm. Since the aim is using light to manipulate particles, their position should be restrained to the illuminated volume, and therefore the width/height of the layer containing particles should be similar to the modal field diameter of the optical waveguide guiding light which will exert the optical gradient/scattering force. Consequently, a flow rate ratio of 0.005 was used (in both the horizontal and vertical HFF devices) as it focuses the particles down to a width/height of 5-10 µm. Higher focusing ratios would increase the width/height of the focal spot, whereas smaller focusing ratios are not possible due to limitations imposed by the syringe pump. Further, to obtain a flow rate ratio of 0.005, flow rates of 0.05 µL/min (sample flow) and 10 µL/min (total sheath flow) were used; larger sample and sheath flow rates would increase the particle velocity, making imaging of the particles, and eventually optical trapping, more difficult, the latter due to higher Stokes drag force. Still, it should be noted that the ideal flow rate ratio depends on the geometry and dimensions of the microfluidic channel, and on the viscosity of the sample and sheath fluids.

Lastly, we highlight that the designed 3D geometry is difficult to fabricate through conventional lithographic techniques given the requirement to machine the bulk of the material.

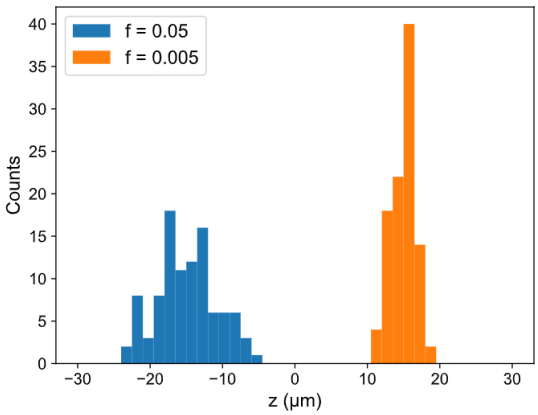

Fig. 9. Histogram of the position of the PS particles along the channel's height for f=0.05 and f=0.005, centered at z =-15 and 15 µm, respectively. The particle solution flow rate was q = 0.05 µL/min for both histograms.

3.2 Dual-Beam Optical Trap

The optical trapping process is made using the capabilities of fs-laser micromachining to integrate both optical waveguides and microfluidic channels. Since the waveguides can be written perpendicular to the fabricated channel, it is possible to create a dual-counter-propagating-Gaussian beam. To understand the origin of the optical trap, we first discuss the effect of a

single waveguide on the microparticle. Given the diameter of the microparticles (3 µm) is larger than the light wavelength (1.55 µm), a particle in the path of one light beam experiences a gradient force pulling it toward the beam axis and a scattering force pushing it away from the light source. Here, with two opposing and identical divergent beams, a microparticle becomes trapped at the point of symmetry (point where resultant scattering force is null), with any displacement from this centre leading to a restoring force. Consequently, inside the channel, a trapping region is created due to the two beams coming out of the integrated optical waveguides. It should also be highlighted that the particle velocity should also be small (≈10 µm/s), otherwise the Stokes drag force can be stronger than the exerted optical force, preventing optical trapping.

The optofluidic device shown in fig. 3 was tested using 3 µm PS particles. Figure 10 shows the obtained results. First with light coming from only one of the waveguides, it was possible to see that a displacement of the particles was induced due to the radiation pressure of a 1550 nm beam coming out of the integrated waveguide. Afterwards, with light coming from both waveguides, a dual-beam trap (1550 nm) derived from the two counter-propagating Gaussian beams coming out of the integrated waveguides was created [20]. It was possible to perform optical trapping with this technique for particles flowing around the same height as the waveguides (fig. 10).

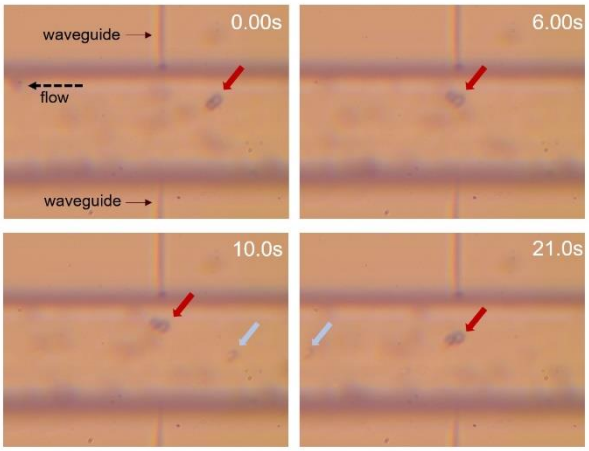

Fig. 10. Snapshots illustrating the effect of the two counter propagating Gaussian beams creating a dual-beam trap for two in-focus PS particles (red arrow). Out-of-focus particles' trajectory (light blue arrow) is not affected by the beams.

These results show our capability of performing both optical trapping and displacement due to pressure radiation on PS microparticles in an integrated monolithic device, which is crucial for the development of cell sorters and stretchers. However, this preliminary study has also proved that with such small channel widths (~36 µm) the flow rate needs to be around 1 nL/min in order to image the particles, which places several restrictions in the syringe pumps stability. Further, even though the channel was small, particles were still randomly distributed over it. Therefore, some of the particles were unaffected by the propagating light beams, which prevents their analysis. A more efficient solution would be to replace this channel by the previously described flow focusing geometries; this is currently under study.

4 Conclusion

On-silica chip 2D HFF devices, in both vertical and horizontal directions, were fabricated through fs-laser direct writing followed by chemical etching. The first tests, performed with red food dye, show that the dimensions of the focused sample stream follow the expected behaviour predicted by Lee *et al,* and can be controlled by adjusting the sample and sheath flow rates. Further tests with 3 µm PS particles show that, with a flow rate ratio of 0.005, the particles could be focused within a 6 µm layer across a 420 µm wide channel, and in a 5 µm layer across a 260 µm high channel.

Light induced movement through pressure radiation and optical trapping of microparticles was also demonstrated by integrating optical waveguides within the microfluidic chip. With this technology, further optical functions can be included for cell sensing by fluorescence detection or light scattering analysis. Combination with the previous HFF geometry can be used for single-line particle focusing near the optical waveguide depth, which paves the way for efficient single particle/cell analysis.

This project is co-financed by Component 5 – Capitalization and Business Innovation, integrated in the Resilience Dimension of the Recovery and Resiliency Plan within the scope of the Recovery and Resilience Mechanism (MRR) of the European Union (EU), framed in the Next Generation EU, for the period 2021-2026 within the scope of the HfPT project with reference 4.

References

1. S. K. Vashist, P. B. Luppa, L. Y. Yeo, A. Ozcan, J. H. Luong, Emerging Technologies for Next-Generation Point-of-Care Testing. Trends in Biotechnology, **33**, 692-705 (2015).
2. D. Tan, K. N. Sharafudeen, Y. Yue, J. Qiu, Femtosecond laser induced phenomena in transparent solid materials: Fundamentals and applications. Progress in Materials Science, **76**, 154-228 (2016).
3. R. Osellame, Femtosecond laser micromachining: photonic and microfluidic devices in transparent materials (Berlin: Springer, 2012)
4. G. Testa, G. Persichetti, R. Bernini, Optofluidic biosensing: devices, strategies, and applications. TrAC Trends in Analytical Chemistry, 117865 (2024).
5. P. Paiè, *et al*, Structured-light-sheet imaging in an integrated optofluidic platform. Lab on a Chip, **24**, 34-46 (2024).
6. N. Bellini, *et al*, Femtosecond laser fabricated monolithic chip for optical trapping and stretching of single cells. Optics Express, **18**, 4679-4688 (2010).

7. J. Qi, *et al*, A microfluidic mixer of high throughput fabricated in glass using femtosecond laser micromachining combined with glass bonding. Micromachines, **11**, 213 (2020).
8. A. A. Al-Halhouli, W. Al-Faqheri, B. Alhamarneh, L. Hecht, A. Dietzel, Spiral microchannels with trapezoidal cross section fabricated by femtosecond laser ablation in glass for the inertial separation of microparticles. Micromachines, **9**, 171 (2018).
9. F. Bragheri, *et al*, Optofluidic integrated cell sorter fabricated by femtosecond lasers. Lab on a Chip, **12**, 3779-3784 (2012).
10. P. Paiè, F. Bragheri, R. M. Vazquez, R. Osellame, Straightforward 3D hydrodynamic focusing in femtosecond laser fabricated microfluidic channels. Lab on a Chip, **14**, 1826-1833 (2014).
11. F. Storti, S. Bonfadini, L. Criante, Simplified 3D hydrodynamic flow focusing for lab-on-chip single particle study. Scientific Reports, **13**, 14671 (2023).
12. J. M. Maia, V. A. Amorim, D. Viveiros, P. V. S. Marques, Femtosecond laser micromachining of an optofluidics-based monolithic whispering-gallery mode resonator coupled to a suspended waveguide. Scientific reports, **11**, 9128 (2021).
13. F. He, Y. Cheng, Z. Xu, Y. Liao, J. Xu, H. Sun, H., X. Chen, Direct fabrication of homogeneous microfluidic channels embedded in fused silica using a femtosecond laser. Optics letters, **35**, 282-284 (2010).
14. J. Drs, T. Kishi, Y. Bellouard, Laser-assisted morphing of complex three dimensional objects. Optics express, **23**, 17355-17366 (2015).
15. D. Ting, Thermofluids: from nature to engineering (Academic Press, 2022)
16. G. B. Lee, C. C. Chang, S. B. Huang and R. J. Yang, The hydrodynamic focusing effect inside rectangular microchannels. Journal of Micromechanics and Microengineering, **16**, 1024 (2006).
17. S. Kendig, Use of microchannels to determine diffusion of food coloring in water. Microelectronics Processing Technology Fall Term (2003).
18. D. Rusu, D. Genoe, P. van Puyvelde, E. Peuvrel-Disdier, P. Navard, G. G. Fuller, Dynamic light scattering during shear: measurements of diffusion coefficients. Polymer, **40**, 1353-1357 (1999).
19. C. Kunstmann-Olsen, J. D. Hoyland, H. G. Rubahn, Influence of geometry on hydrodynamic focusing and long-range fluid behavior in PDMS microfluidic chips. Microfluidics and nanofluidics, **12**, 795-803 (2012).
20. J. M. Taylor, Counter-Propagating Gaussian Beam Traps. Optical Binding Phenomena: Observations and Mechanisms (Springer Theses, 2011).